[4] K. F. Casey, "On the effective impedance of thin coaxial cable shields," *IEEE Trans. Electromagn. Compat.*, vol. EMC-18, pp. 110–117, Aug. 1976.
[5] J. R. Wait and D. A. Hill, "Influence of spatial dispersion of the shield transfer impedance of a braided coaxial cable," *IEEE Trans. Microwave Theory Tech.*, vol. MTT-25, pp. 72–74, Jan. 1977.
[6] J. R. Wait, "Quasi-static limit for the propagating mode along a thin wire in a circular tunnel," *IEEE Trans. Antennas Propagat.*, vol. AP-25, pp. 441–443, May 1977.
[7] A. D. Wheelon, *Tables of Summable Series and Integrals Involving Bessel Functions*. San Francisco: Holden-Day, 1968, p. 44.
[8] R. E. Collin, *Field Theory of Guided Waves*. New York: McGraw-Hill, 1960, p. 124.
[9] J. Fontaine, B. Demoulin, P. Degauque, and R. Gabillard, *Proc. of the Thru-the-Earth Electromagnetics Workshop*, U.S. Bureau of Mines, Aug. 1973 (available from the National Technical Information Service, 5285 Port Royal Road, Springfield, VA 22152, Document No. PB 231 154).

Electromagnetic Transmission Through a Filled Slit in a Conducting Plane of Finite Thickness, TE Case

DAVID T. AUCKLAND, STUDENT MEMBER, IEEE, AND ROGER F. HARRINGTON, FELLOW, IEEE

Abstract—**A solution is developed for computing the transmission characteristics of a slit in a conducting screen of finite thickness placed between two different media. The slit may be filled with lossy material while the two regions on either side of the screen are assumed lossless. A magnetic line source excitation is used (TE case) which is parallel to the axis of the slit. The equivalence principle is invoked to replace the two slit faces by equivalent magnetic current sheets on perfect electric conductors. Two coupled integral equations containing the magnetic currents as unknowns are then obtained and solved for by the method of moments. Pulses are used for the expansion and testing functions. Quantities computed are equivalent magnetic currents, the transmission coefficient, the gain pattern, and the normalized far field pattern.**

I. Introduction

THE PROBLEM of diffraction of plane waves through a slit in a perfect electric conductor of finite thickness has been studied by several investigators [1]–[5]. The most extensive investigation was that of Lehman [1], who used the analytic properties of finite Fourier transforms. The solution of Kashyap and Hamid [2] used a Wiener–Hopf and generalized matrix technique. Both of these solutions were done for the TM case (incident electric field parallel to slit axis). The solutions of Hongo [3] and of Neerhoff and Mur [4], were obtained by a numerical solution of coupled integral equations and were done for the TE case. A similar solution for the TM case was obtained by Wirgin [5]. In this paper, we use the method of moments to solve coupled integral equations similar in form to those derived in [4].

Manuscript received November 28, 1977; revised February 10, 1978. This work was supported by the National Science Foundation, Washington, DC, under Grant ENG 76-04588.

The authors are with the Department of Electrical and Computer Engineering, Syracuse University, Syracuse, NY 13210.

This paper utilizes the generalized network formulation of coupling through apertures developed in [6] and [7] and extends these results to three regions coupled by two apertures. To accomplish this the equivalence principle is used to replace both faces of the slit by perfect conductors, each of which carry magnetic current sheets on both sides. The original problem is now broken up into three regions which are coupled by the postulated magnetic current sheets. The two half-space regions are loss free with arbitrary μ and ϵ and the medium in the slit is assumed lossy with arbitrary complex μ and ϵ.

Continuity of the tangential magnetic field is used to derive two coupled operator equations involving the equivalent magnetic currents as unknowns. These equations are put into matrix form using the method of moments, and solved by using standard matrix methods. The result can be interpreted in terms of a combination of "admittance matrices" computed separately for each region. This gives rise to a network interpretation of the problem which treats the unknown magnetic currents as port voltages and the excitation as port currents.

II. Problem Formulation

The original problem configuration is shown in Fig. 1. It consists of a perfect electric conductor of thickness d separating two regions a and c which may have different electrical properties. Coupling between the two regions occurs through a slit of width w filled with an arbitrarily lossy medium. The conductor is infinite in the z and y directions. The problem consists of three regions separated by two boundaries (the slit faces). Using the equivalence principle, the three regions can be separated by

0018-9480/78/0700-0499$00.75

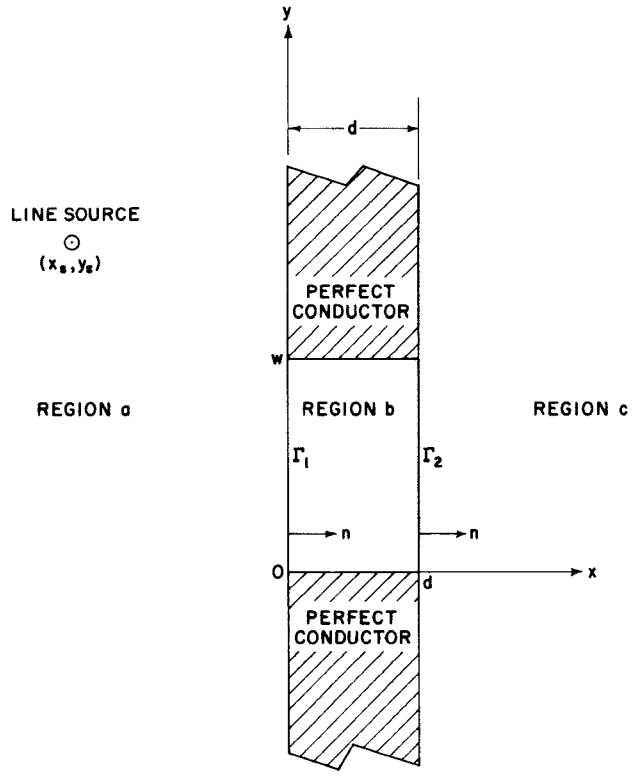

Fig. 1. Original problem.

covering the slits with perfect electric conductors and magnetic currents, as described in [6].

The regions are defined as:

$$\begin{aligned} &\text{region } a \quad x<0, \text{ all } y \\ &\text{region } b \quad 0<x<d,\ 0<y<w \\ &\text{region } c \quad x>d, \text{ all } y \end{aligned}$$

and the boundaries as:

$$\begin{aligned} &\Gamma_1 \quad x=0,\ 0<y<w \\ &\Gamma_2 \quad x=d,\ 0<y<w \end{aligned}$$

which are the two boundaries of separation. To utilize the equivalence principle, Γ_1 and Γ_2 are covered by perfect electric conductors, and on each side of these conductors a magnetic current sheet is placed which is determined by

$$\boldsymbol{M}_1 = \boldsymbol{n} \times \boldsymbol{E}_1, \qquad \text{on } \Gamma_1 \tag{1a}$$

$$\boldsymbol{M}_2 = \boldsymbol{E}_2 \times \boldsymbol{n}, \qquad \text{on } \Gamma_2 \tag{1b}$$

where $\boldsymbol{E}_1$ and $\boldsymbol{E}_2$ are the total electric fields in the aperture at Γ_1 and Γ_2, respectively. This breaks the original problem up into three parts as shown in Fig. 2. The magnetic current sheets on each side of Γ_1 and Γ_2 are equal and opposite in sign for each slit face because in the actual problem the tangential electric field must be continuous across them. Enforcing the condition that the total tangential magnetic field is continuous across Γ_1 and Γ_2 leads to two coupled operator equations [11]

$$\boldsymbol{H}_{t1}^a(\boldsymbol{M}_1) + \boldsymbol{H}_{t1}^b(\boldsymbol{M}_1) + \boldsymbol{H}_{t1}^b(\boldsymbol{M}_2) = -\boldsymbol{H}_t^i \tag{2a}$$

$$\boldsymbol{H}_{t2}^b(\boldsymbol{M}_1) + \boldsymbol{H}_{t2}^b(\boldsymbol{M}_2) + \boldsymbol{H}_{t2}^c(\boldsymbol{M}_2) = 0. \tag{2b}$$

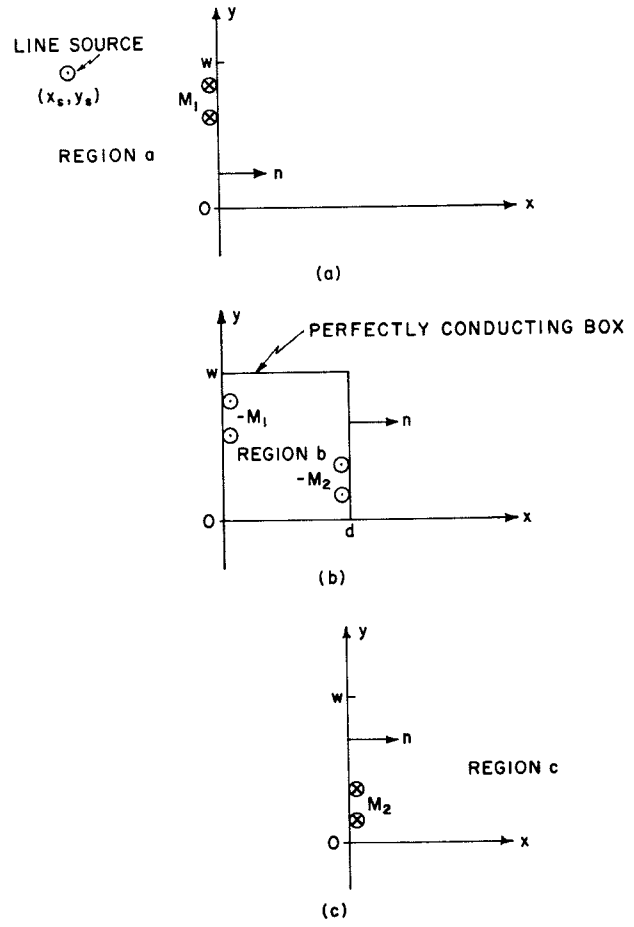

Fig. 2. Equivalences for regions *a*, *b*, and *c*.

In the above, $\boldsymbol{H}_t^i$ is the tangential component of the incident magnetic field at Γ_1, $\boldsymbol{H}_{t1}^a$, and $\boldsymbol{H}_{t2}^c$ are the fields of equivalent sources, all in the presence of a complete conductor. $\boldsymbol{H}_{t1}^b$ and $\boldsymbol{H}_{t2}^b$ are the fields of equivalent sources radiating inside a closed two dimensional conducting box. Also the subscripts $t1$ and $t2$ mean the tangential components at Γ_1 or Γ_2, respectively.

Equations (2a) and (2b) must be solved simultaneously and we apply the method of moments. Assuming the magnetic current sheets may be expanded in a linear combination of basis functions defined on Γ_1 and Γ_2 we have

$$\boldsymbol{M}_1 = \sum_{n=1}^{N_1} V_{1n} \boldsymbol{M}_{1n}, \qquad \text{on } \Gamma_1 \tag{3a}$$

$$\boldsymbol{M}_2 = \sum_{n=1}^{N_2} V_{2n} \boldsymbol{M}_{2n}, \qquad \text{on } \Gamma_2. \tag{3b}$$

Here V_{1n} and V_{2n} are unknown complex scalars and $\boldsymbol{M}_{1n}$ and $\boldsymbol{M}_{2n}$ are vector basis functions on Γ_1 and Γ_2 defined by

$$\boldsymbol{M}_{1n} = \begin{cases} 1\boldsymbol{u}_z, & (n-1)\Delta y \leqslant y \leqslant n\Delta y \\ 0, & \text{elsewhere} \end{cases} \tag{4}$$

for $n = 1, 2, \cdots, N_1$ and $y = w/N_1$, y being on Γ_1. $\boldsymbol{M}_{2n}$ is defined exactly the same but with y now on Γ_2. The usual

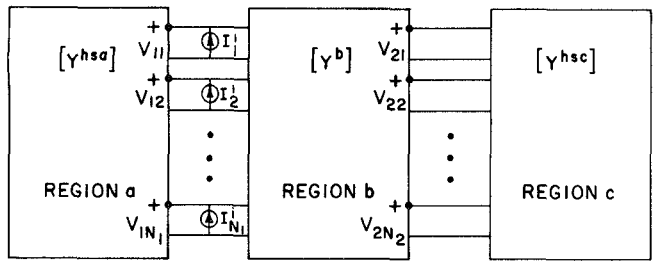

Fig. 3. Network representation for (6).

symmetric product

$$\langle X, Y\rangle = \int_{\Gamma_1 \cup \Gamma_2} \boldsymbol{X}\cdot\boldsymbol{Y}\,dy \tag{5}$$

is used where the variable of integration is either on Γ_1 or Γ_2. The testing functions $\boldsymbol{W}_{1m}$ and $\boldsymbol{W}_{2m}$ are the same as the vector basis functions defined by (4). Taking the symmetric product of (2a) with $\boldsymbol{W}_{1m}$ and (2b) with $\boldsymbol{W}_{2m}$, we obtain in matrix form

$$\begin{aligned}[Y^{hsa}+Y^{11}]\bar{V}_1+[Y^{12}]\bar{V}_2&=\bar{I}^i\\ [Y^{21}]\bar{V}_1+[Y^{22}+Y^{hsc}]\bar{V}_2&=\bar{O}.\end{aligned} \tag{6}$$

Here the various component matrices are explicitly identified by

$$[Y^{hsa}] = -\left[\langle W_{1m}, H_{t1}^a(M_{1n})\rangle\right]_{N_1\times N_1} \tag{7a}$$

$$[Y^{hsc}] = -\left[\langle W_{2m}, H_{t2}^c(M_{2n})\rangle\right]_{N_2\times N_2} \tag{7b}$$

$$[Y^{11}] = -\left[\langle W_{1m}, H_{t1}^b(M_{1n})\rangle\right]_{N_1\times N_1} \tag{7c}$$

$$[Y^{12}] = -\left[\langle W_{1m}, H_{t1}^b(M_{2n})\rangle\right]_{N_1\times N_2} \tag{7d}$$

$$[Y^{21}] = -\left[\langle W_{2m}, H_{t2}^b(M_{1n})\rangle\right]_{N_2\times N_1} \tag{7e}$$

$$[Y^{22}] = -\left[\langle W_{2m}, H_{t2}^b(M_{2n})\rangle\right]_{N_2\times N_2} \tag{7f}$$

$$\bar{I}^i = \left[\langle W_{1m}, H_t^i\rangle\right]_{N_1\times 1}. \tag{7g}$$

Equation (6) composes a $(N_1+N_2)\times(N_1+N_2)$ system of linear equations which suggests the network representation shown in Fig. 3, where

$$[Y^b] = \begin{bmatrix} [Y^{11}] & [Y^{12}] \\ [Y^{21}] & [Y^{22}] \end{bmatrix}. \tag{8}$$

The matrices $[Y^{hsa}]$, $[Y^b]$, and $[Y^{hsc}]$ are the network representations of regions a, b, and c, respectively. The explicit computation of these quantities which, to carry the network analogy further we call admittance matrices, depends only upon their respective regions.

Since the expansion and testing functions are identical it is clear from (7c) through (7f) that

$$\begin{aligned}[Y^{11}]&=[\tilde{Y}^{11}]\\ [Y^{21}]&=[\tilde{Y}^{12}]\\ [Y^{22}]&=[\tilde{Y}^{22}]\end{aligned} \tag{9}$$

where the tilda ($\tilde{}$) denotes the matrix transpose. Also, for simplicity, we take $N_1=N_2=N$ and note that

$$\begin{aligned}[Y^{11}]&=[Y^{22}]\\ [Y^{21}]&=[Y^{12}].\end{aligned} \tag{10}$$

III. Computation of Matrix Elements

The admittance matrices for regions a and c are quite simple to compute. For example, in region a, $\boldsymbol{H}_{t1}^a(\boldsymbol{M}_{1n})$ gives the field of current sheet $\boldsymbol{M}_{1n}$ radiating into the half space a in the presence of a complete conductor. Thus we have

$$\boldsymbol{H}_{t1}^a(\boldsymbol{M}_{1n}) = -\frac{k_a}{2\eta_a}\int_{\Gamma_1} \boldsymbol{M}_{1n} H_0^{(2)}(k_a|y-y'|)\,dy' \tag{11}$$

where $k_a=\omega\sqrt{\mu_a\epsilon_a}$, $\eta_a=\sqrt{\mu_a/\epsilon_a}$, ω=radian frequency of line source, and $H_0^{(2)}$ is the Hankel function of second kind, order zero. Substituting (4) for $\boldsymbol{M}_{1n}$ and using the fact that $\boldsymbol{W}_{1m}=\boldsymbol{M}_{1m}$ for $m=1,2,\cdots,N$ we have for the mnth element of (7a):

$$Y_{mn}^{hsa} = \frac{k_a}{2\eta_a}\int_{\Delta y_m}\int_{\Delta y_n} H_0^{(2)}(k_a|y-y'|)\,dy\,dy'. \tag{12}$$

Here Δy_m is the region on Γ_1 where $W_{1m}\neq 0$ and Δy_n is the region on Γ_1 where $\boldsymbol{M}_{1n}\neq 0$. The admittance matrix for region c is exactly the same as (12) except with subscript a replaced by c. It is also evident that $[Y^{hsa}]$ and $[Y^{hsc}]$ are symmetric Toeplitz matrices and hence only one column of each need be computed [12].

The elements of $[Y^b]$ are given by (7c) through (7f). For the TE case under consideration all the magnetic currents are z directed. Thus an electric vector potential function $\boldsymbol{F}$ can be defined in region b as [8]

$$\boldsymbol{F}=\psi\boldsymbol{u}_z \tag{13}$$

where ψ is a scalar wave potential satisfying the two dimensional differential equation

$$\frac{\partial^2\psi}{\partial x^2}+\frac{\partial^2\psi}{\partial y^2}+k_b^2\psi=0 \tag{14}$$

everywhere in region b except where the sources $\boldsymbol{M}_1$ or $\boldsymbol{M}_2$ exist. The wave propagation constant in region b is $k_b=\omega\sqrt{\mu_b\epsilon_b}$ and is in general a complex number. The fields are found from $\boldsymbol{F}$ by

$$\begin{aligned}\boldsymbol{E}&=-\nabla\times\boldsymbol{F}\\ \boldsymbol{H}&=-j\omega\epsilon_b\boldsymbol{F}.\end{aligned} \tag{15}$$

Now to compute $[Y^{11}]$ and $[Y^{21}]$, we need $\boldsymbol{H}_{t1}^b(\boldsymbol{M}_{1n})$ and $\boldsymbol{H}_{t2}^b(\boldsymbol{M}_{1n})$ where the boundary conditions on ψ are

$$\begin{aligned}\left.\frac{\partial\psi}{\partial y}\right|_{y=0,w} &= \left.\frac{\partial\psi}{\partial x}\right|_{x=d} = 0\\ \left.\frac{\partial\psi}{\partial x}\right|_{\Gamma_1} &= -\boldsymbol{M}_{1n}.\end{aligned} \tag{16}$$

The solution to (14) satisfying (16) is given by

$$\psi = \sum_{p=0}^{\infty} A_p \cos k_{xp}(x-d)\cos\frac{p\pi y}{w} \tag{17}$$

where $k_{xp}^2 = k_b^2 - (p\pi/w)^2$,

$$A_p = \frac{-\epsilon_p}{wk_{xp}\sin k_{xp}d}\int_0^w M_{1n}\cos\frac{p\pi y}{w}\,dy \tag{18}$$

and ϵ_p is Neumann's number ($\epsilon_p = 1$ for $p=0$ and $\epsilon_p = 2$ for $p>0$). Thus from (7c) and (7e) we obtain the mnth elements of $[Y^{11}]$ and $[Y^{21}]$:

$$Y_{mn}^{11} = -\frac{j\omega\epsilon_b}{w}\sum_{p=0}^{\infty}\frac{\epsilon_p\cot k_{xp}d}{k_{xp}} \cdot\int_{\Gamma_1}\int_{\Gamma_1} M_{1n}W_{1m}\cos\frac{p\pi y'}{w}\cos\frac{p\pi y}{w}\,dy\,dy'$$

$$Y_{mn}^{21} = -\frac{j\omega\epsilon_b}{w}\sum_{p=0}^{\infty}\frac{\epsilon_p\csc k_{xp}d}{k_{xp}} \cdot\int_{\Gamma_2}\int_{\Gamma_1} M_{1n}W_{2m}\cos\frac{p\pi y'}{w}\cos\frac{p\pi y}{w}\,dy\,dy'. \tag{19}$$

The elements of $[Y^{12}]$ and $[Y^{22}]$ are found from (10). More detailed derivation of these equations is given in [11].

The tangential component of incident magnetic field $\boldsymbol{H}_t^i$ is given by

$$\boldsymbol{H}_t^i = -\boldsymbol{u}_z\frac{k_aK}{2\eta_a}H_0^{(2)}(k_aR_s) \tag{20}$$

where $R_s = \sqrt{x_s^2+(y-y_s)^2}$ and K is the strength of the line source. Substitution of (20) into (7g) yields for the mth element of the excitation vector $\bar{I}^i$:

$$I_m^i = -\frac{k_aK}{2\eta_a}\int_{\Delta y_m}H_0^{(2)}(k_aR_s)\,dy. \tag{21}$$

The variable of integration is on Γ_1. Equation (6) may now be solved for $\bar{V}_1$ and $\bar{V}_2$.

IV. Transmission Coefficient

The transmission coefficient of the slit is defined as the ratio of the time average power transmitted into region c by the slit P_{trans} to the time average incident power intercepted by the slit from region a P_{inc}, both for a unit length in the z direction. The usual formula for power flow into the network represented by $[Y^{hsc}]$ of Fig. 3 gives

$$P_{\text{trans}} = \text{Re}\,\tilde{V}_2[Y^{hsc}]^*\bar{V}_2^* \tag{22}$$

where $*$ denotes a complex conjugate. P_{inc} is that portion of the time average power radiated into whole space per unit length by a magnetic line source of strength K which is intercepted by the aperture. It is given by

$$P_{\text{inc}} = \frac{\theta k_a}{8\pi\eta_a}|K|^2 \tag{23}$$

where θ is the angle subtended by the aperture, as defined in Fig. 4. Thus the formula for the transmission coefficient is

$$T = \frac{8\pi\eta_a}{\theta k_a|K|^2}\text{Re}\{\tilde{V}_2[Y^{hsc}]^*\bar{V}_2^*\}. \tag{24}$$

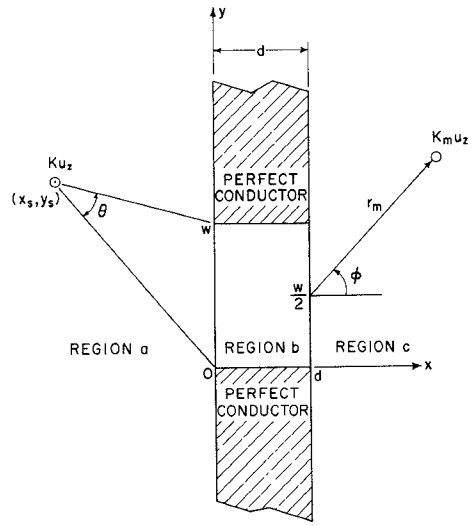

Fig. 4. Geometry used in computing transmission coefficient and measurement of H_m at r_m.

V. Power Gain and Measurement Vector

The power gain pattern in region c is defined as the ratio of the radiation intensity in a given direction to the radiation intensity which would exist if the transmitted time average power were radiated over half space, or

$$G(\phi) = \frac{\pi r_m\eta_c|H_m|^2}{P_{\text{trans}}}. \tag{25}$$

Here, H_m is the component of the magnetic field in region c in the direction of a magnetic test line current $K_m\boldsymbol{u}_z$ due to current $\boldsymbol{M}_2$ radiating in the presence of a complete conductor at $x=d$. $K_m\boldsymbol{u}_z$ is used to measure H_m at position (r_m,ϕ) by reciprocity. If $\boldsymbol{H}_K^i$ is the field at Γ_2 due to $K_m\boldsymbol{u}_z$ radiating in the presence of a complete conductor, we obtain from reciprocity

$$H_mK_m = \int_{\Gamma_2}\boldsymbol{H}_K^i\cdot\boldsymbol{M}_2\,dy. \tag{26}$$

After using (3b) and rewriting the result in matrix form, we have

$$H_mK_m = \tilde{I}^m\bar{V}_2 \tag{27}$$

where $\tilde{I}^m$ is the tranpose of a measurement vector defined as

$$\bar{I}^m = [\langle M_{2n}, H_K^i\rangle]_{N\times 1}. \tag{28}$$

The elements of $\bar{I}^m$ are given by

$$I_n^m = -\frac{k_cK_m}{2\eta_c}\int_0^w \boldsymbol{M}_{2n}\cdot\boldsymbol{u}_zH_0^{(2)}\left(k_c\left|\boldsymbol{r}_m+\left(\frac{w}{2}-y\right)\boldsymbol{u}_y\right|\right)dy. \tag{29}$$

If $r_m \gg \lambda_c$ (far field measurements), where $\lambda_c = 2\pi/k_c$, then (29) becomes

$$I_n^m = \int_0^w M_{2n}e^{jk_c(y-(w/2))\sin\phi}\,dy \tag{30}$$

where K_m is adjusted to

$$\frac{1}{K_m} = -\frac{1}{\eta_c}\sqrt{\frac{jk_c}{2\pi r_m}}\,e^{-jk_cr_m}. \tag{31}$$

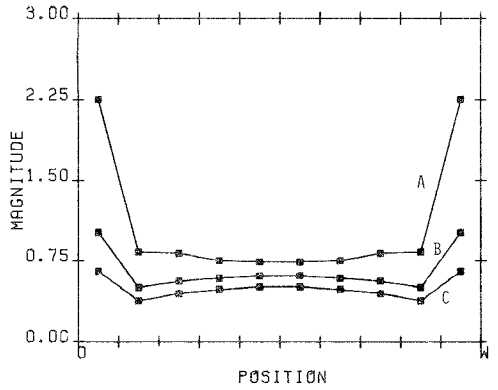

Fig. 5. Magnitude of M_1 (squares) and M_2 (triangles) for slit $w=0.4\lambda_a$, $d=0.001\lambda_a$, $k_b=k_a=k_0$. A is $\epsilon_c=\epsilon_0$, B is $\epsilon_c=5\epsilon_0$, and C is $\epsilon_c=10\epsilon_0$. $N=10$.

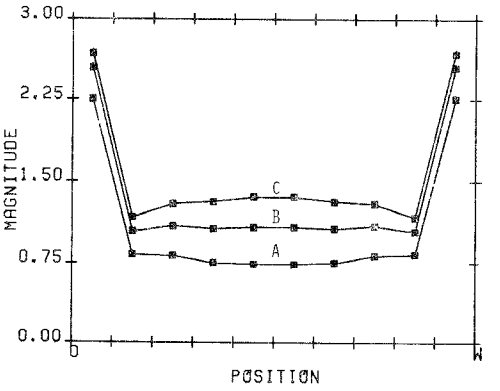

Fig. 6. Magnitude of M_1 (squares) and M_2 (triangles) for slit $w=0.4\lambda_a$, $d=0.001\lambda_a$, $k_b=k_a=k_0$. A is $\mu_c=\mu_0$, B is $\mu_c=3\mu_0$, and C is $\mu_c=10\mu_0$. $N=10$.

The measured component of magnetic field is now given by

$$H_m=-\frac{1}{\eta_c}\sqrt{\frac{jk_c}{2\pi r_m}}\,e^{-jk_c r_m}\left\{\tilde{I}^m\bar{V}_2\right\} \tag{32}$$

and the final formula for power gain is

$$G(\phi)=\frac{k_c}{2\eta_c P_{\text{trans}}}\left|\tilde{I}^m\bar{V}_2\right|^2 \tag{33}$$

VI. Numerical Examples

All the examples presented here are done with the magnetic line source at a distance of one hundred wavelengths in region a from the center of the slit face Γ_1 and the strength adjusted so that the incident electric field at the center of Γ_1 is equal to unity. The source is at normal incidence except where noted. Figs. 5 and 6 show the magnitudes of magnetic currents computed for a relatively thin slit ($w=0.4\lambda_a$, $d=0.001\lambda_a$) for different values of permittivity and permeability in region c when regions a and b are free space. As expected, $M_1=-M_2$ to within the third or fourth significant figure, the minus sign denoting 180° phase difference. Also, when $d=0$, the agreement is quite good between results in Fig. 5 and those computed in [9].

Two examples done by Neerhoff and Mur [4] for a slit with $w=1\mu$, $d=0.1\mu$, and $\lambda_0=0.4353\mu$ appear in Fig. 7

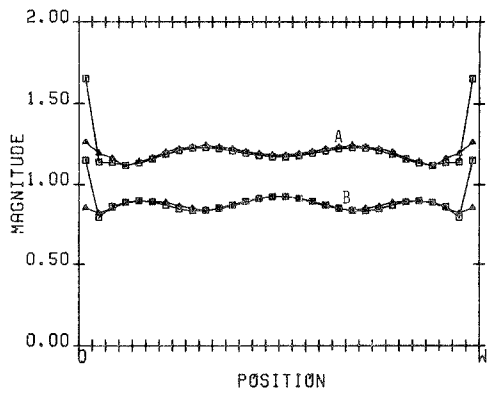

Fig. 7. Magnitudes of M_2 for $w=1\mu$, $d=0.1\mu$, $\lambda_0=0.4353\mu$, A is $k_a=1.5k_o$, $k_c=k_b=k_o$, and B is $k_a=1.5k_o$, $k_c=1.6k_o$, $k_b=k_o$. Triangles represent values taken from [4] and squares represent values obtained from our computations. $N=30$.

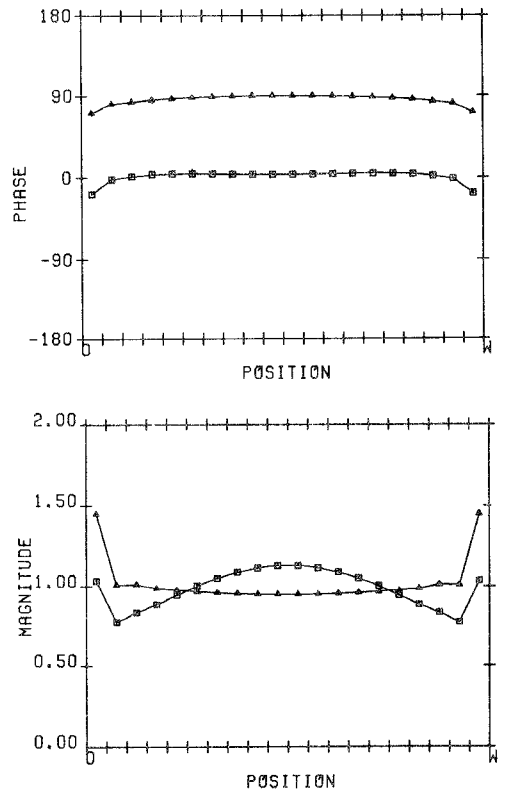

Fig. 8. Magnitude and phase of M_1 (squares) and M_2 (triangles) for $\epsilon_a=\epsilon_b\epsilon_c=\epsilon_o$, $d=0.25\lambda_a$, $w=1\lambda_a$. $N=20$.

when region b is free space and regions a and c have different permittivities. The magnitudes of currents M_2 obtained from our solution and from [4] are compared and agreement is quite good except at the very end point where the edge singularity behavior is dominant. Figs. 8 through 10 show the effects of having a lossy medium in region b for a slit with $w=1\lambda_a$, $d=0.25\lambda_a$ when regions a and c are free space.

Fig. 11 shows gain and normalized field patterns for a slit with varying thickness and different values of ϵ_b. Our results agree well with the same example computed in [4]. These cases were also experimentally measured in [10]. There are slight discrepancies in the magnitudes of the sidelobes and nulls when the measured results are compared with computed results.

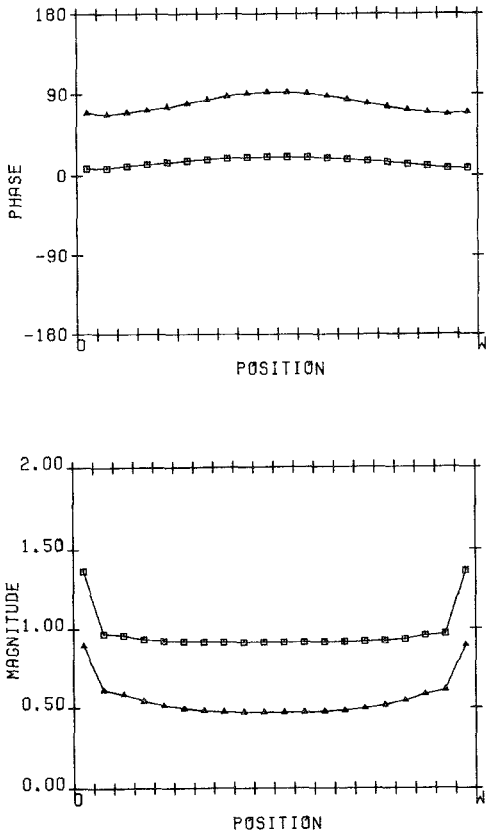

Fig. 9. Magnitude and phase of M_1 (squares) and M_2 (triangles) for $\epsilon_a = \epsilon_c = \epsilon_o$, $d = 0.25\lambda_a$, $w = 1\lambda_a$, and $\epsilon_b = (1 - j)\epsilon_o$. $N = 20$.

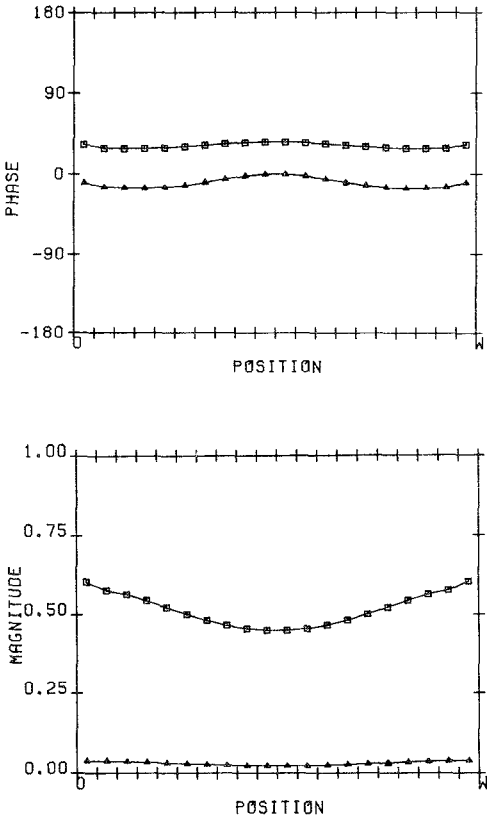

Fig. 10. Magnitude and phase of M_1 (squares) and M_2 (triangles) for $\epsilon_a = \epsilon_c = \epsilon_o$, $d = 0.25\lambda_a$, $w = 1\lambda_a$, and $\epsilon_b = (1 - j10)\epsilon_o$. $N = 20$.

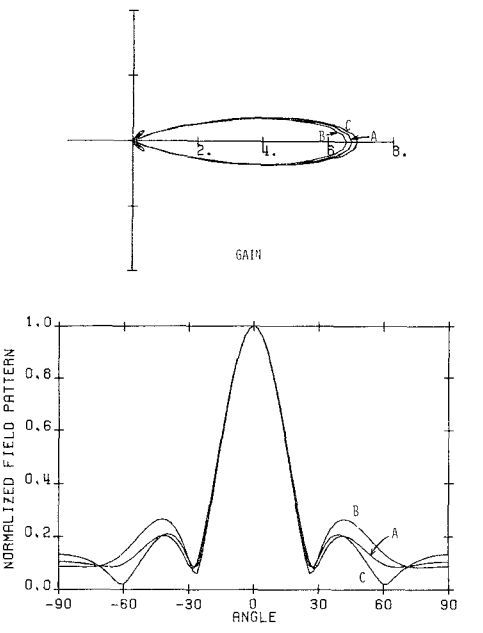

Fig. 11. Gain and normalized field patterns for $k_a = k_c = k_o$, $w = 2.148\lambda_a$. A is $d = 0.0417\lambda_a$, $\epsilon_b = \epsilon_o$. B is $d = 1.331\lambda_a$, $\epsilon_b = \epsilon_o$. C is $d = 1.331\lambda_a$, $\epsilon_b = 2.59\epsilon_o$. $N = 30$.

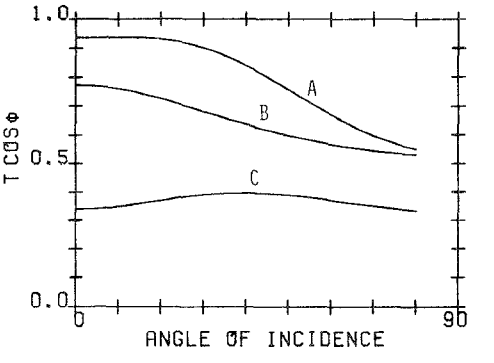

Fig. 12. Plots of transmission coefficient times $\cos\phi$ versus ϕ, where ϕ is the angle of incidence of the line source measured from the negative x axis, for $w = 0.8\lambda_a$, $d = 0.25\lambda_a$, $k_a = k_c = k_o$. A is $\epsilon_b = \epsilon_o$, B is $\epsilon_b = 5\epsilon_o$, and C is $\epsilon_b = 10\epsilon_o$. $N = 10$.

Fig. 12 shows the effect on the transmission coefficient for a slit with $w = 0.8\lambda_a$, $d = 0.25\lambda_a$ as the source is placed at different angles of incidence (as measured from the negative x axis). The quantity actually plotted is the time-average power transmitted by the slit divided by the time-average power incident upon Γ_1 when the source is at normal incidence. This amounts to simply multiplying (24) by $\cos\phi$, where ϕ is the angle of incidence. This gives a transmission coefficient equivalent to that computed in [13] and [14] for $d = 0$. Finally Fig. 13 is a plot of $T\cos\phi$ versus ϕ for two very thin slits. These are the same as results obtained when $d = 0$ given in [13] and [14].

VII. Discussion

The generalized network formulation of coupling through apertures developed in [6] and [7] has been extended to three regions coupled by two apertures. By using the equivalence principle, a straightforward formulation of transmission through a slit in a screen of

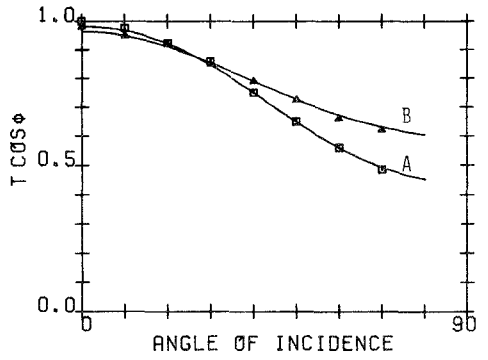

Fig. 13. Plots of transmission coefficient times $\cos\phi$ versus ϕ, where ϕ is the angle of incidence of the line source as measured from the negative x axis, for $k_a = k_b = k_c$. A is $w = 1.02\lambda_a$, $d = 10^{-5}\lambda_a$, and B is $w = 0.51\lambda_a$, $d = 10^{-4}\lambda_a$. Squares and triangles represent values taken from the results in [13] for $d = 0$. $N = 10$.

finite thickness has been developed. Though the problem formulation is inherently simple, the solution of (6) is not free of computational difficulties. For instance, the matrix $[Y^b]$ becomes ill-conditioned as $d \to 0$, even though it may be shown [11] that this formulation reduces to that given in [6] for the case where $d = 0$. In the actual computations, however, fairly small values of d may be used (i.e., $d = 10^{-4}w$ or $10^{-5}w$). Also if medium b is lossless and the slit dimensions w or d are such that

$$\left(\frac{p}{w}\right)^2 + \left(\frac{q}{d}\right)^2 = \left(\frac{2}{\lambda_b}\right)^2 \tag{34}$$

is satisfied for integers p, q, some terms of $[Y^b]$ become infinite and our numerical solution fails. A seemingly reliable solution, however, may be obtained for these "resonant" cases by slightly perturbing the dimensions w or d, or by adding a slight amount of loss to region b. The actual computation of $[Y^b]$ and a documented computer program are described in [11].

References

[1] G. W. Lehman, "Diffraction of electromagnetic waves by planar dielectric structures. I. Transverse Electric Excitation," *Journal of Math. Physics*, vol. 11, pp. 1522–1535, May 1970.

[2] S. C. Kashyap and M. A. K. Hamid, "Diffraction characteristics of a slit in a thick conducting screen," *IEEE Trans. Antennas Propagat.*, vol. AP-19, pp. 499–507, July 1971.

[3] Kohei Hongo, "Diffraction of electromagnetic plane waves by infinite slit perforated in a conducting screen with finite thickness," *Elec. Comm.* (Japan), vol. 54-B, pp. 90–96, 1971.

[4] F. L. Neerhoff and G. Mur, "Diffraction of a plane electromagnetic wave by a slit in a thick screen placed between two different media," *Appl. Sci. Res.*, vol. 28, pp. 73–88, July 1973.

[5] A. Wirgin, "Influence de l'épaisseur de l'écran sur la diffraction par une fente," *C. R. Acad. Sc. Paris*, t. 270, Série B, pp. 1457–1460, June 8, 1970.

[6] R. F. Harrington and J. R. Mautz, "A generalized network formulation for aperture problems," *IEEE Trans. Antennas Propagat.*, vol. AP-24, pp. 870–873, Nov. 1976.

[7] ——, "Electromagnetic transmission through an aperture in a conducting plane," *AEU*, vol. 31, pp. 81–87, Feb. 1977.

[8] R. F. Harrington, *Time-Harmonic Electromagnetic Fields*. New York: McGraw-Hill, 1961, Sec. 3–12.

[9] C. M. Butler and K. R. Umashankar, "Electromagnetic penetration through an aperture in an infinite, planar screen separating two half spaces of different electromagnetic properties," *Radio Sci.*, vol. 11, pp. 611–619, July 1976.

[10] S. C. Kashyap, *et al.*, "Diffraction pattern of a slit in a thick conducting screen," *J. Appl. Phys.*, vol. 42, pp. 894–895, Feb. 1971.

[11] D. T. Auckland and R. F. Harrington, "Electromagnetic transmission through a filled slit in a conducting plane of finite thickness, TE Case," Report TR-77-9, Dept. of Electrical and Computer Engineering, Syracuse University, Syracuse, NY 13210, Sept. 1977.

[12] D. H. Preis, "The Toeplitz matrix: Its occurrence in Antenna Problems and a rapid inversion algorithm," *IEEE Trans. Antennas Propagat.*, vol. AP-20, pp. 204–205, Mar. 1972.

[13] P. M. Morse and P. J. Rubenstein, "The diffraction of waves by ribbons and by slits," *Phys. Rev.*, vol. 54, pp. 895–898, Dec. 1938.

[14] Y. T. Chou and A. T. Adams, "The coupling of electromagnetic waves through long slots," *IEEE Trans. Electromagn. Compat.*, vol. EMC-19, pp. 65–73, May 1977.